Published in final edited form as:
Ann Biomed Eng. 2011 January ; 39(1): 287–296. doi:10.1007/s10439-010-0127-y.

Electrochemical Impedance Spectroscopy to Assess Vascular Oxidative Stress

Fei Yu[1], **Rongsong Li**[1], **Lisong Ai**[1], **Collin Edington**[1], **Hongyu Yu**[2], **Mark Barr**[3], **E. S. Kim**[4], and **Tzung K. Hsiai**[1]

[1]Department of Biomedical Engineering and Cardiovascular Medicine, University of Southern California, Los Angeles, CA 90089, USA

[2]School of Earth & Space Exploration, Arizona State University, Tempe, AZ 85287-8406, USA

[3]Department of Cardiothoracic Surgery, University of Southern California, Los Angeles, CA, USA

[4]Department of Electrical Engineering and Electrophysics, University of Southern California, Los Angeles, CA, USA

Abstract

Vascular inflammatory responses are intimately linked with oxidative stress, favoring the development of pre-atherosclerotic lesions. We proposed that oxidized low density lipoprotein (oxLDL) and foam cell infiltrates in the subendothelial layer engendered distinct electrochemical properties that could be measured in terms of the electrochemical impedance spectroscopy (EIS). Concentric bipolar microelectrodes were applied to interrogate EIS of aortas isolated from fat-fed New Zealand White (NZW) rabbits and explants of human aortas. Frequency-dependent EIS measurements were assessed between 10 kHz and 100 kHz, and were significantly elevated in the pre-atherosclerotic lesions in which oxLDL and macrophage infiltrates were prevalent (At 100 kHz: aortic arch lesion = 26.7 ± 2.7 kΩ vs. control = 15.8 ± 2.4 kΩ; at 10 kHz: lesions = 49.2 ± 7.3 kΩ vs. control = 27.6 ± 2.7 kΩ, $n = 10$, $p<0.001$). Similarly, EIS measurements were significantly elevated in the human descending aorta where pre-atherosclerotic lesions or fatty streaks were prominent. EIS measurements remained unchanged in spite of various depths of electrode submersion or orientation of the specimens. Hence, the concentric bipolar microelectrodes provided a reliable means to measure endoluminal electrochemical modifications in regions of pro-inflammatory with high spatial resolution and reproducibility albeit uneven lesion topography and non-uniform current distribution.

Keywords

Electrochemical impedance spectroscopy; Oxidative stress; Atherosclerosis; oxLDL; Endothelium

INTRODUCTION

Oxidized low density lipoprotein (oxLDL) and macrophage infiltrates contribute to pro-inflammatory states relevant to the initiation of atherosclerotic lesions.[37] These lesions can be classified as stable or unstable plaque. The latter is often non-obstructive by conventional X-ray angiography or intravascular ultrasound (IVUS), and is prone to rupture, leading to

Address correspondence to Tzung K. Hsiai, Department of Biomedical Engineering and Cardiovascular Medicine, University of Southern California, Los Angeles, CA 90089, USA. hongyuyu@asu.edu, hsiai@usc.edu.

acute coronary syndromes or stroke.[2,11,21] Unstable plaque or otherwise known as thin-cap fibroatheroma represents a transitional plaque that is characterized by a thin fibrous cap (<65 μm), a large necrotic core, an abundance of macrophages, and limited luminal narrowing. [37] However, detection and diagnosing the non-obstructive, albeit pro-inflammatory, lesions during catheterization remains a clinical challenge.

Up to date, there are no diagnostic tools to detect intravascular oxidative stress and pro-inflammatory states when patients undergo angiograms. Serum biomarkers have been proposed for predicting pro-inflammatory states. Examples include C-reactive protein, matrix metalloproteinases, CD40 ligand, Lp-PLA_2 (lipoprotein-associated phospholipase A_2) and myelo-peroxidase. Specifically, circulating Lp-PLA_2 is bound predominantly to low-density lipoprotein (LDL) (~80%) which transmigrated to the subendothelial space of atherosclerosis-prone regions.[28] Imaging modalities including magnetic resonance imaging (MRI) and electron beam computed tomography (EBCT) have also been proposed to predict unstable plaque.[7,29] However, assessing stable vs. unstable atherosclerotic lesions during catheterization remains an unmet clinical need.

Atherosclerotic lesions display distinct electrochemical properties.[34,35] Pre-atherosclerotic lesions harbor pro-inflammatory substrates; namely, oxLDL and macrophage-derived foam cells infiltrates, which engender distinct endoluminal electrochemical impedance or otherwise quantified as electrochemical impedance spectroscopy (EIS).[19,34] Previously, changes in bulk resistance were prevalent in the atherosclerotic lesions as measured by the linear 4-point probe.[19,34,35] Electric impedance (Z) develops as a function of frequency in response to the applied alternative current (AC) to the biological tissue. Recently, a catheter-based linear 4-point microelectrode was reported to assess EIS in New Zealand White (NZW) rabbits.[19,34,35] In our study, we introduced concentric bipolar microelectrodes to further address the non-uniform and complex tissue current distribution, uneven endoluminal topography and non-uniform current distribution, in both rabbit aortas and human descending aortas. Our findings indicate the potential application of concentric bipolar microelectrodes to measure electrochemical impedance in regions of pro-inflammatory states with high spatial resolution.

MATERIALS AND METHODS

Rabbit Aortas and Explants of Human Descending Aortas

Two male NZW rabbits (10-week-old) were acquired from a local breeder (Irish Farms, Norco, CA) and maintained by the USC vivaria in accordance with the National Institutes of Health guidelines. After a 7-day quarantine period, they were fed with a high-fat, high-cholesterol diet (Newco® 1.5% cholesterol and 6% peanut oil) for 8 weeks. The rabbits were then euthanized with an overdose of intramuscular injection of ketamine (Fort Dodge Laboratories, Inc) combined with 1 mg/kg Acepromazine (Aveco Co.). The hearts and aorta were resected for *ex vivo* study and immunohistochemistry. All experimental procedures were performed in compliance with the Institutional Animal Care and Use Committee in the Heart Institute of the Good Samaritan Hospital, Los Angeles, which is accredited by the American Association for Accreditation for Laboratory Animal Care.

Also, six explants of human descending aortas and common carotid arteries were collected from cardiac transplant patients or National Disease Research Interchange (NDRI) for study in compliance with the University Institutional Review Board.

Operating Principle and Equivalent Circuit Model

Electrical impedance (*Z*) is a measure of the opposition to electrical flow through a substance, a complex quantity combining resistance and reactance as a function of frequency

when an AC was applied. The value of impedance is conventionally represented as a complex number ($Z = R + iX_c$), consisting of the real number R for the resistance and the complex number iX_c for the reactance.[3] Blood vessels harbor resistance and store charges, exhibiting complex electric impedances as a function of frequency. Hence, we were able to determine the lesions' frequency-dependent electrical and dielectrical behavior by recording the electric impedance of a tissue over a frequency range.[20]

Biological tissue impedance measured by metallic electrodes entailed electrode–electrolyte interface. Investigations on the electrochemical properties at the interface can be dated to as early as 1871,[13] and various equivalent circuit models have been proposed. To date, a simple yet efficient model for the electrochemical impedance in tissue is represented as a parallel interface capacitance impedance, C_P, shunted by a charge transfer resistance, R_P, in series with the tissue resistance, R_S (Fig. 1a).[3] A more sophisticated model replaces C_P with a constant phase angle impedance Z_{CPA} (Fig. 1b), a measurement for the non-Faraday impedance arising from the interface capacitance and non-homogeneities,[10] which can be expressed by the empirical relation:

$$Z_{CPA} = \frac{1}{(j\omega Q)^n} \quad (1)$$

with n being a constant ($0<n<1$) for the nonhomogeneities of the surface and ω being angular frequency equal to $2\pi f$. If $n = 1$, the Q is equal to C_P, and Z_{CPA} represents a purely capacitive impedance element corresponding to the interface capacitance. [10,23] In the case of concentric bipolar electrode experiments (Fig. 1c), the R_S is mainly dependent on the tissue composition and the geometric dimension of the tissue between the inner working electrode and the outer counter electrode, whereas the R_P and Z_{CPA} are predominantly dependent on the tissue dielectric and conductive properties as well as the geometric dimension between the two electrodes.

Ex vivo Electrochemical Impedance Spectroscopy Measurements

The rabbit aorta was flushed with physiological saline solution and resected longitudinally to expose the inner lumen. Tissue specimens at approximately 2 cm in length were isolated from the aortic arch, thoracic aorta, and abdominal aorta, respectively. Gross histology of atherosclerotic lesions was identified for the individual specimens (Fig. 2). For the human artery specimens, *en face* arteries were sectioned longitudinally to reveal endoluminal surface. Two specimens were observed to have mild to prevalent fatty streaks (Fig. 3). The tissues were maintained in the phosphate buffered saline (PBS).

Endoluminal EIS measurements were performed at multiple sites associated with the plaque lesions and compared to the healthy arterial lumens and to PBS. More than three replicates were performed at each site. The concentric bipolar microelectrodes (FHC Co., ME, USA) consisted of working and reference electrodes; the former was the inner pole made of the platinum at 75 μm in diameter, and the latter was the stainless steel outer shell made of a at 300 μm in diameter. An Ag/AgCl electrode immersed in the PBS solution was used as a reference electrode. EIS measurements were performed by using a Gamry Series G 300 potentiostat (Gamry Instruments, PA) installed in a Dell desktop computer. An input of 10 mV peak-to-peak AC voltage and a frequency decay ranging from 300 kHz to 100 Hz were delivered to the sites. The magnitudes and phases of the impedance were acquired at 20 data points per frequency decade. To test whether the depth of PBS solution and orientation of contact with the specimens would interfere with the EIS recordings, we mounted the concentric bipolar microelectrode on a micro-manipulator (World Precision Instruments Inc., FL, USA). EIS measurements were performed at the identical point of interest for the

electrodes submersed in four various depths in PBS solution while in contact with the specimen, or the specimens were rotated around the electrodes by 90°.

Immunohistochemistry

Vascular rings or stripes were cut from the rabbit aorta or human artery immediately after the specimens were collected and measured, and immersed in 4% paraformaldehyde for 24 h. They were then frozen in optical cutting temperature compound (Sakura Finetek, Torrance, CA) for histopathological analysis. Serial 5-μm cryosections were cut. Immunostaining was performed with standard techniques in frozen vascular tissue using biotinylated secondary antibodies and streptavidin-conjugated horse radish peroxidase (HRP). Chromogen Diaminobenzidine (DAB) was used as the substrate of HRP, and the sections were counterstained with hematoxylin for the visualization of intima, media, smooth muscle cells, and adventitia. Plaque macrophages, or foam cells, were identified. Tissue sections were viewed with a microscope (Leica DM LB2, Leica Microsystems, Germany), and images were captured with a CCD digital camera (Spot RT-KE, Diagnostic Instruments, MI, USA). Evaluation of the plaque histology was performed according to the modified AHA classification of atherosclerotic lesions.[32–34,39] For further evaluation of the local oxidation stress, foam cells were identified by Sudan black stain,[15,16,38] macrophages with anti-CD68 antibody, and oxLDL with mAb4E6.[15] H&E and von Kossa staining were used to demonstrate calcification. A color intensity threshold mask for immunostaining was defined to detect foam cells and oxLDL.

Statistical Analysis

Histological plaque characteristics were qualitatively ranked in four groups (no/minor/moderate/severe oxidative stress). Statistical analyses were performed using two-tailed *T*-test for two groups of data, or one-way ANOVA for multi-group comparison with the statistical software package SPSS 15.0 (SPSS Inc., Chicago, IL). p values of less than 0.05 were considered statistically significant. Power analysis determined sample size (N) for rabbits.

RESULTS

Endoluminal EIS Measurements at Various Microelectrode Submersion and Tissue Orientation

En face segments of rabbit aorta revealed prevalent pre-atherosclerotic lesions. After 8 weeks of high-fat diet, pre-atherosclerotic lesions were prominent in the aortic arch in which disturbed flow occurred (Fig. 2a), whereas the segment distal to the aortic arch was spared of visible lesions (Fig. 2b). Next, EIS measurements were performed in relation to the depth of microelectrode submersion and orientation of the specimens. Both EIS and phase measurements were identical as the electrode was positioned from 0 mm to 4 mm below PBS solution surface (Fig. 4a). At 300 kHz, the lowest impedance was measured at ~4000 Ω, corresponding to a phase value of about −15°, indicating near-ohmic resistance. Furthermore, impedance was inversely proportional to the frequencies, indicating the effect of double layer capacitance at the electrode/electrolyte interface. Moreover, EIS measurements were compared at two different sites of the endoluminal surface (Fig. 4b). Both EIS and phase measurements remained unchanged despite rotation of the specimens at 90°. Hence, the impedance readings acquired by the concentric bipolar microelectrodes were unaffected by the depth of electrode submersion and orientation of specimens.

Endoluminal EIS Measurements between Healthy and Atherosclerotic Lesions in Rabbits

Electrochemical impedance spectroscopy measurements were compared between the healthy and atherosclerotic tissues from the two rabbits. Five representative healthy sites and atherosclerotic sites were assessed (from Fig. 2a), and significant differences in EIS measurements were observed between 10 kHz and 100 kHz in the aortic arch (Fig. 5a). Bar graphs further corroborated statistically significant differences in EIS values ($p<0.01$, $n = 10$) (Fig. 5b). The impedances of the lesions were nearly 2-fold higher than those of the healthy sites. Hence, concentric bipolar microelectrodes offered a reliable entry point to assess endoluminal EIS for plaque diagnosis.

Linking Electrochemical Impedance with Immunohistochemistry

We demonstrated EIS measurements in the non-obstructive, albeit pro-inflammatory, pre-atherosclerotic lesions in both aortic arch and descending aortas isolated from the fat-fed rabbits. The pre-atherosclerotic lesions, occupying less than 20% of the luminal diameter, were notable for both intimal thickening and intimal xanthoma (Fig. 6), which corresponded to the EIS measurements as illustrated in Fig. 4. Intimal thickening consisted of mainly smooth muscle cells in a proteoglycan-rich matrix, whereas intimal xanthoma or otherwise known as a fatty streak primarily contained macrophage-derived foam cells (Fig. 6c), T lymphocytes (not stained), and varying degrees of smooth muscle cells (SMC).[39] Intimal thickening further revealed positive staining for oxLDL (Fig. 6d). Calcification was absent as evidenced by the negative von Kossa staining. These lesions possessing minor to medium oxidative stress were considered clinically silent and were previously reported to have no significantly different impedance spectrum compared to healthy aorta.[35] However, concentric bipolar micro-electrodes enabled the detection of endoluminal impedance spectrum changes in the presence of oxLDL and macrophage/foam cell infiltrates.

Linking Electrochemical Impedance with Fatty Streaks in Human Descending Aortas

Fatty streak or otherwise known as early atheromas harbor oxLDL and microphages/foam cell infiltrates.[39] *En face* segments of human descending aorta and carotid arteries revealed numerous fatty streaks for which endoluminal EIS measurements were performed (Fig. 3). Significant differences in EIS measurements were observed between 10 kHz and 100 kHz in the descending aortas (Figs. 7a and 8a). Bar graphs further corroborated statistically significant differences in EIS values (Figs. 7b and 8b) ($p<0.05$, $n = 3$, and $p<0.01$, $n = 6$, respectively). The impedances of the fatty streaks were nearly 1.5-fold higher than those of the healthy sites. Immunohistochemistry analysis revealed presence of oxLDL (Figs. 8c and 8d) in the lesion region. Hence, endoluminal EIS measurements provided distinct electrochemical impedance in regions properties of pre-atheromas from explants of human arteries.

DISCUSSION

To better characterize the biochemical properties of non-obstructive, albeit pro-inflammatory, lesions, we demonstrated the application of endoluminal EIS. EIS measures the dielectric properties of a specimen as a function of frequency.[5] It is based on the interaction of an external field with the electric dipole moment of the samples, often expressed by permittivity.[26] The novelty of this study was to address biological tissues that harbor both energy storing and dissipation properties. The configuration of concentric bipolar microelectrodes allowed for consistent and reliable electrical impedance measurement despite the non-homogeneous composition and non-uniform current distribution in the lesions.

We showed that EIS measurements were significantly elevated in the pre-atherosclerotic lesions or otherwise known as fatty streaks or deposition in which oxLDL and macrophage/foam cell infiltrates were prevalent. Thus, linking endoluminal EIS measurements with pre-atherosclerotic lesions holds promise to develop intravascular-based sensors and to predict pro-inflammatory lesions when the patients are undergoing catheterization.

The use of a linear array of four microelectrodes based on microfibrication and semiconductor technology was recently reported.[34] A balloon catheter system with an integrated polyiminde-based micro-electrode structure was introduced into the aorta, and the impedance was measured at frequency range 1–10 kHz. Then the corresponding histomorphometric data of the aortic segments were compared.[35] The investigators provided the first catheter-based four-point electrodes arranged axially with a diameter of 100 μm and a spacing of 333 μm apart for impedance measurement in the NZW rabbits on high-fat diet.

Unlike the linear array of electrodes, concentric configuration further allowed for EIS measurement independent of the depth of the PBS submersion and orientation of the tissues. Electrical currents flow preferably via the least resistive pathways; that is, the shortest conducting paths between the central electrode and the outer shell of the concentric bipolar microelectrodes. Owing to the micro-scale of the concentric electrodes, the impedance measurement is mainly sensitive to the electrochemical properties of the tissue at close proximity, and changes in volume of saline solution would not alter the impedance reading. Our *ex vivo* investigation can be extrapolated to perform *in vivo* investigation in which the impedance measurements will be independent of lumen diameters, blood volumes, and flow rates as long as the contact is made between microelectrodes and endoluminal surface.

Up to date, little is known about the numerous variables affecting assessment of atherosclerotic lesions. Investigations have been centered around atherosclerotic lesion's lipid pool content, calcification, fibrous cap, and intima/media thickness.[11] The emerging vascular oxidative hypothesis of unstable plaque is that atherosclerotic lesion is deemed a dynamic process.[8,14] Reactive oxygen species via NADPH oxidase enzyme system and the release of matrix metalloproteinase (MMP) by the inflammatory cells contribute to the vulnerability of a rupture-prone plaque.[12] These macrophage-derived foam cells are trapped by interaction with oxLDL and can be mobilized by dynamic exposure in response to key antioxidants such as apocynin, *N*-acetylecysteine (NAC), as well as resveratrol, a polyphenolic compound in grapes and red wine.[27]

In this study, we focused on the specific content of oxidative stress; namely, oxLDL and foam cell infiltrates, and assessed both aortas of NZW rabbits and explants of human arteries. The ability to obtain reliable EIS measurements with high special resolution provides a basis to further deploy the catheter-based concentric bipolar microelectrodes for endoluminal EIS assessment *in vivo*. Ideally, EIS sensors can be incorporated onto a steerable catheter accompanied with intravascular ultrasound (IVUS) to scan the circumferential profile of the atherosclerotic.[24] In fact, EIS measurement can be performed at multiple sites for a single lesion to generate a contour map containing both topographical and electrochemical information. In addition, EIS measurements can be potentially incorporated with intracardiac echocardiogram, [22] optical coherence tomography (OCT),[17,40] and/or micro-thermal sensors[1] to further enhance the sensitivity and specificity for the assessment of pro-inflammatory states or unstable plaque.

Distinct from the linear four-point electrode arrays, our methodology employed the concentric bipolar electrodes (FHC®), allowing for reproducible assessment for vascular regions harboring vascular oxidative stress in terms of oxLDL and foam cells.[18] The unique feature of the concentric electrodes included the constant and symmetric displacement

between the working and counter electrodes. Similar to the previously reported EIS,[34,35] specimens that harbor oxidative stress generated distinctly higher EIS values compared to the healthy tissues over a range of frequency from 10 kHz to 100 kHz. Moreover, the EIS measurements were independent of the surrounding medium and orientation of the specimens.

Severe stenosis reduces arterial blood flow and causes high tensile and compressive stress in the stenotic plaque.[36] Oxidative stress and pro-inflammatory states modulate mechanical vulnerability of plaque.[30] Oxidative stress is involved in the oxidation/modification of low-density lipoprotein,[4,6,41] which occurs at high levels in the atherogenic prone regions of aorta and plays a critical role in pro-inflammatory states.[25] Mounting evidence supports that oxLDL and macrophage/foam cell-rich shoulder areas are more prone to disruption, leading to thrombus formation and embolic events.[9] Hence, the application of EIS to assess pre-atherosclerotic lesions will likely provide a means to measure electrochemical properties in regions of pro-inflammatory states that harbor both oxLDL and foam cells. Further characterization of EIS in relation to histology is warranted to stratify the extent of oxidative stress and pro-inflammatory states to identify patients in whom selective intervention may be indicated.

In summary, we demonstrated a link between electrochemical properties and vascular oxidative stress in the pre-atherosclerotic lesions in the aortas of NZW rabbits and explants of human descending aortas. These distinct electrochemical properties of the lesions correlated with the substrates of vascular oxidative stress; namely, oxLDL and macrophage/foam cell infiltrates. It has been demonstrated that the fat present in the plaques has high specific electrical resistivity compared to other possible plaque compounds.[31] Atheromas at various stages contain differential levels of lipid-rich components, rendering a differential level of oxidative stress that can be potentially identified by the magnitude of tissue impedance.

Acknowledgments

This study was supported by AHA Pre-Doctoral Fellowship 0615063Y (L. A.), NHLBI HL 83015 (T. K. H.), and NHLBI HL091302 (T. K. H.). We thank Dr. P. Holvoet of the Catholic University of Leuven, Belgium for providing us the oxLDL antibody.

References

1. Ai L, Yu H, Dai W, Hale SL, Kloner RA, Hsiai TK. Real-time intravascular shear stress in the rabbit abdominal aorta. IEEE Trans Biomed Eng. 2009; 56(6):1755–1764. [PubMed: 19527952]
2. Ambrose JA, Tannenbaum MA, Alexopoulos D, Hjemdahl-Monsen CE, Leavy J, Weiss M, Borrico S, Gorlin R, Fuster V. Angiographic progression of coronary artery disease and the development of myocardial infarction. Lead Article. 1988; 12:184–202.
3. Aroom KR, Harting MT, Cox CS, Radharkrishnan RS, Smith C, Gill BS. Bioimpedance analysis: a guide to simple design and implementation. J Surg Res. 2009; 153(1):23–30. [PubMed: 18805550]
4. Asatryan L, Hamilton R, Mario Isas J, Hwang J, Kayed R, Sevanian A. LDL phospholipid hydrolysis produces modified electronegative particles with an unfolded apoB-100 protein. J Lipid Res. 2005; 46:115–122. [PubMed: 15489541]
5. Barsoukov, E.; Macdonald, JR. Impedance spectroscopy: theory, experiment, and applications. Malden, MA: Wiley-Interscience; 2005.
6. Berliner JA, Heinecke JW. The role of oxidized lipoprotein in atherogenesis. Free Radic Biol Med. 1996; 20(5):707–727. [PubMed: 8721615]
7. Choudhury RP, Fuster V, Badimon JJ, Fisher EA, Fayad ZA. MRI and characterization of atherosclerotic plaque: emerging applications and molecular imaging. Arterioscler Thromb Vasc Biol. 2002; 22(7):1065–1074. [PubMed: 12117718]

8. Curtiss LK. Reversing atherosclerosis. N Engl J Med. 2009; 360:1144–1146. [PubMed: 19279347]
9. Ehara S, Ueda M, Naruko T, Haze K, Itoh A, Otsuka M, Komatsu R, Matsuo T, Itabe H, Takano T, Tsukamoto Y, Yoshiyama M, Takeuchi K, Yoshikawa J, Becker AE. Elevated levels of oxidized low density lipoprotein show a positive relationship with the severity of acute coronary syndromes. Circulation. 2001; 103(15):1955–1960. [PubMed: 11306523]
10. Franks W, Schenker I, Schmutz P, Hierlemann A. Impedance characterization and modeling of electrodes for biomedical applications. IEEE Trans Biomed Eng. 2005; 52(7):1295–1302. [PubMed: 16041993]
11. Fuster V, Badimon L, Badimon JJ, Chesebro JH. The pathogenesis of coronary artery disease and the acute coronary syndromes. N Eng J Med. 1992; 326(4):242–250.
12. Galis ZS. Vulnerable plaque: the devil is in the details. Circulation. 2004; 110(3):244–246. [PubMed: 15262853]
13. Geddes LA. Historical evolution of circuit models for the electrode-electrolyte interface. Ann Biomed Eng. 1997; 25(1):1–14. [PubMed: 9124725]
14. Heistad DD. Unstable coronary-artery plaques. N Eng J Med. 2003; 349(24):2285–2287.
15. Holvoet P, Vanhaecke J, Janssens S, Van de Werf F, Collen D. Oxidized LDL and malondialdehyde-modified LDL in patients with acute coronary syndromes and stable coronary artery disease. Circulation. 1998; 98(15):1487–1494. [PubMed: 9769301]
16. Holvoet P, Mertens A, Verhamme P, Bogaerts K, Beyens G, Verhaeghe R, Collen D, Muls E, Van de Werf F. Circulating oxidized LDL is a useful marker for identifying patients with coronary artery disease. Arterioscler Thromb Vasc Biol. 2001; 21(5):844–848. [PubMed: 11348884]
17. Jang IK, Bouma BE, Kang DH, Park SJ, Park SW, Seung KB, Choi KB, Shishkov M, Schlendorf K, Pomerantsev E. Visualization of coronary atherosclerotic plaques in patients using optical coherence tomography: comparison with intravascular ultrasound. J Am Coll Cardiol. 2002; 39(4): 604–609. [PubMed: 11849858]
18. Kolodgie FD, Katocs ASJ, Largis EE, Wrenn SM, Cornhill JF, Herderick EE, Lee SJ, Virmani R. Hypercholesterolemia in the rabbit induced by feeding graded amounts of low-level cholesterol. Methodological considerations regarding individual variability in response to dietary cholesterol and development of lesion type. Arterioscler Thromb Vasc Biol. 1996; 16(12):1454–1464. [PubMed: 8977449]
19. Konings MK, Mali W, Viergever MA. Development of an intravascular impedance catheter for detection of fatty lesions in arteries. IEEE Trans Med Imaging. 1997; 16(4):439–446. [PubMed: 9263001]
20. Foster KR, Schwan HP. Dielectric properties of tissues. Handbook of biological effects of electromagnetic fields. 1996:25–102.
21. Little WC, Constantinescu M, Applegate RJ, Kutcher MA, Burrows MT, Kahl FR, Santamore WP. Can coronary angiography predict the site of a subsequent myocardial infarction in patients with mild-to-moderate coronary artery disease? Circulation. 1988; 78(5):1157–1166. [PubMed: 3180375]
22. Marrouche NF, Martin DO, Wazni O, Gillinov AM, Klein A, Bhargava M, Saad E, Bash D, Yamada H, Jaber W. Phased-array intracardiac echocardiography monitoring during pulmonary vein isolation in patients with atrial fibrillation: impact on outcome and complications. Circulation. 2003; 107(21):2710–2716. [PubMed: 12756153]
23. McAdams ET, Lackermeier A, McLaughlin JA, Macken D, Jossinet J. The linear and non-linear electrical properties of the electrode-electrolyte interface. Biosens Bioelectron. 1995; 10(1–2):67–74.
24. Nair A, Kuban BD, Tuzcu EM, Schoenhagen P, Nissen SE, Vince DG. Coronary plaque classification with intravascular ultrasound radiofrequency data analysis. Circulation. 2002; 106(17):2200–2206. [PubMed: 12390948]
25. Navab M, Berliner JA, Watson AD, Hama SY, Territo MC, Lusis AJ, Shih DM, Van Lenten BJ, Frank JS, Demer LL, Edwards PA, Fogelman AM. The Yin and Yang of oxidation in the development of the fatty streak. A review based on the 1994 George Lyman Duff Memorial Lecture. Arterioscler Thromb Vasc Biol. 1996; 16(7):831–842. [PubMed: 8673557]
26. Orazem, ME.; Tribollet, B. Electrochemical Impedance Spectroscopy. 2008.

27. Park YM, Febbraio M, Silverstein RL. CD36 modulates migration of mouse and human macrophages in response to oxidized LDL and may contribute to macrophage trapping in the arterial intima. J Clin Invest. 2009; 119(1):136–145. [PubMed: 19065049]
28. Ross R. Atherosclerosis is an inflammatory disease. Am Heart J. 1999; 138(5):S419–S420. [PubMed: 10539839]
29. Schmermund A, Erbel R. Unstable coronary plaque and its relation to coronary calcium. Circulation. 2001; 104(14):1682–1687. [PubMed: 11581149]
30. Schwartz SM, Galis ZS, Rosenfeld ME, Falk E. Plaque rupture in humans and mice. Arterioscler Thromb Vasc Biol. 2007; 27(4):705–713. [PubMed: 17332493]
31. Slager CJ, Phaff AC, Essed CE, Bom N, Schuurbiers JCH, Serruys PW. Electrical impedance of layered atherosclerotic plaques on human aortas. IEEE Trans Biomed Eng. 1992; 39(4):411–419. [PubMed: 1592407]
32. Stary HC. Natural history and histological classification of atherosclerotic lesions: an update. Arterioscler Thromb Vasc Biol. 2000; 20(5):1177–1178. [PubMed: 10807728]
33. Stary HC, Chandler AB, Dinsmore RE, Fuster V, Glagov S, Insull WJ, Rosenfeld ME, Schwartz CJ, Wagner WD, Wissler RW. A definition of advanced types of atherosclerotic lesions and a histological classification of atherosclerosis. Arterioscler Thromb Vasc Biol. 1995; 15(9):1512–1531. [PubMed: 7670967]
34. Streitner I, Goldhofer M, Cho S, Thielecke H, Kinscherf R, Streitner F, Metz J, Haase KK, Borggrefe M, Suselbeck T. Electric impedance spectroscopy of human atherosclerotic lesions. Atherosclerosis. 2009; 206(2):464–468. [PubMed: 19419719]
35. Suselbeck T, Thielecke H, Kochlin J, Cho S, Weinschenk I, Metz J, Borggrefe M, Haase KK. Intravascular electric impedance spectroscopy of atherosclerotic lesions using a new impedance catheter system. Basic Res Cardiol. 2005; 100(5):446–452. [PubMed: 15795794]
36. Tang D, Yang C, Kobayashi S, Zheng J, Vito RP. Effect of stenosis asymmetry on blood flow and artery compression: a three-dimensional fluid-structure interaction model. Ann Biomed Eng. 2003; 31(10):1182–1193. [PubMed: 14649492]
37. Vengrenyuk Y, Carlier S, Xanthos S, Cardoso L, Ganatos P, Virmani R, Einav S, Gilchrist L, Gilchrist L, Gilchrist L, Weinbaum S. A hypothesis for vulnerable plaque rupture due to stress-induced debonding around cellular microcalcifications in thin fibrous caps. Proc Natl Acad Sci USA. 2006; 103(40):14678–14683. [PubMed: 17003118]
38. Verhamme P, Quarck R, Hao H, Knaapen M, Dymarkowski S, Bernar H, Van Cleemput J, Janssens S, Vermylen J, Gabbiani G, Kockx M, Holvoet P. Dietary cholesterol withdrawal reduces vascular inflammation and induces coronary plaque stabilization in miniature pigs. Cardiovasc Res. 2002; 56(1):135–144. [PubMed: 12237174]
39. Virmani R, Kolodgie FD, Burke AP, Farb A, Schwartz SM. Lessons from sudden coronary death: a comprehensive morphological classification scheme for atherosclerotic lesions. Arterioscler Thromb Vasc Biol. 2000; 20(5):1262–1275. [PubMed: 10807742]
40. Yabushita H, Bouma BE, Houser SL, Aretz HT, Jang IK, Schlendorf KH, Kauffman CR, Shishkov M, Kang DH, Halpern EF. Characterization of human atherosclerosis by optical coherence tomography. Circulation. 2002; 106(13):1640–1645. [PubMed: 12270856]
41. Yamaguchi Y, Haginaka J, Morimoto S, Fujioka Y, Kunitomo M. Facilitated nitration and oxidation of LDL in cigarette smokers. Eur J Clin Invest. 2005; 35(3):186–193. [PubMed: 15733073]

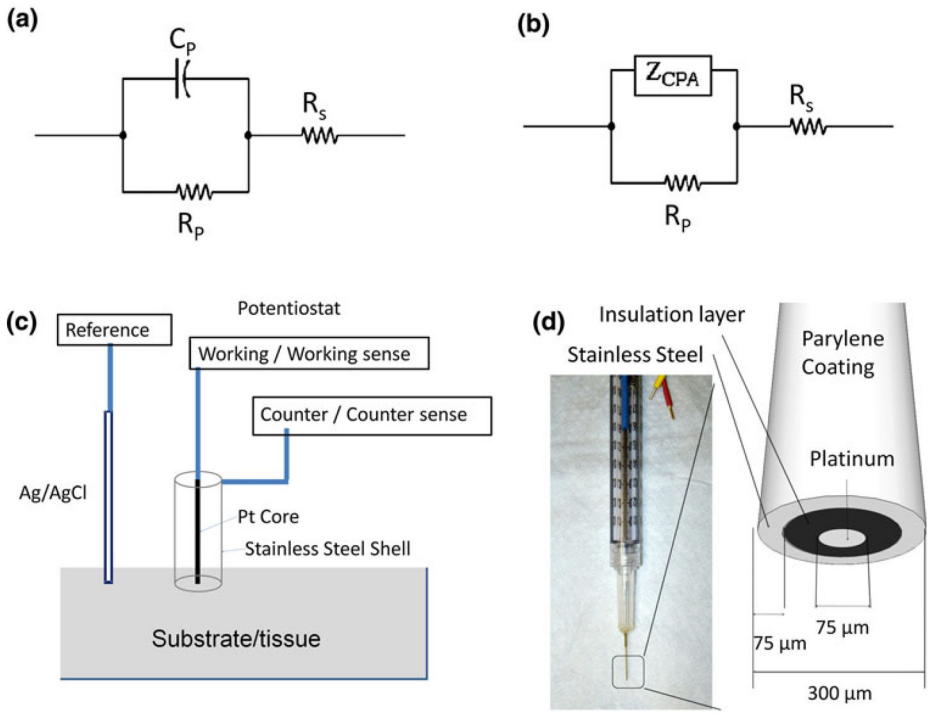

FIGURE 1.

(a) Equivalent circuit model of electrode–tissue interface, with interface reactance represented by a single capacitor C_P. R_P: charge transfer resistance, R_S: Tissue/electrolyte resistance. (b) Equivalent circuit model of electrode–tissue interface, with interface reactance represented by a constant phase element (Z_{CPA}). (c) Illustration of experimental setup. Ag/AgCl reference electrode, Platinum core of the concentric bipolar electrode, and Stainless steel outer shell of the bipolar electrode were connected to the potentiostat as the reference, working, and counter electrode, respectively. (d) Illustration of the geometry and dimension of the bipolar electrode tip.

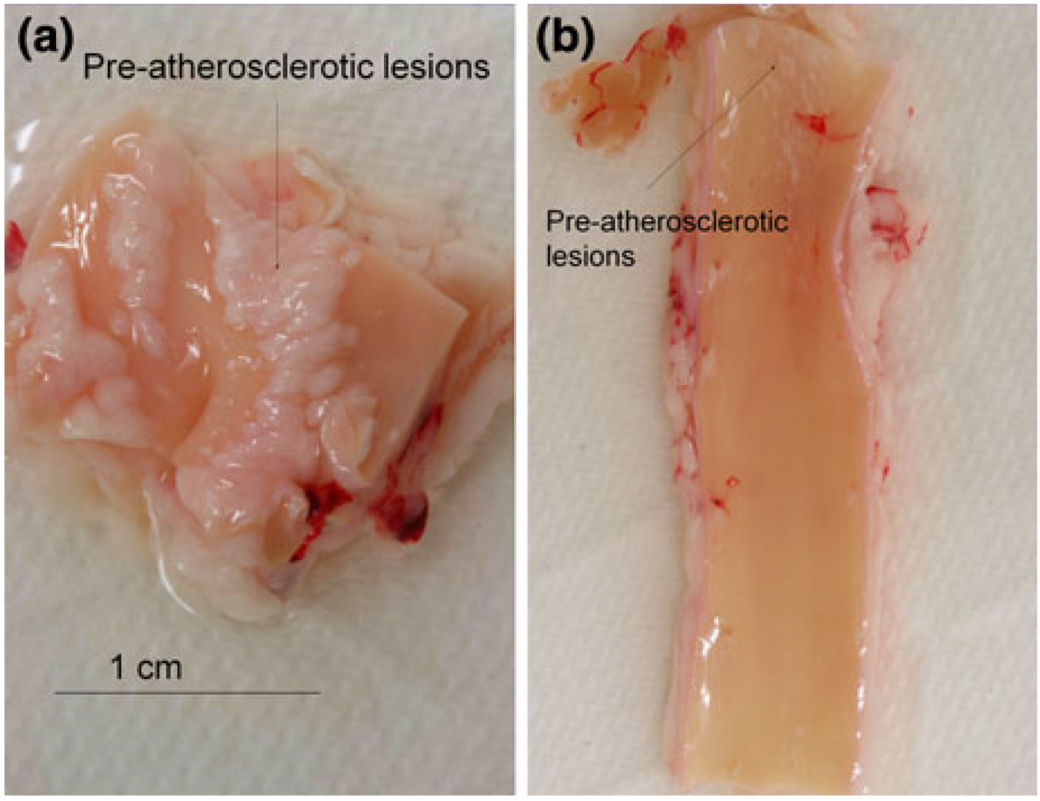

FIGURE 2.

Rabbit aorta in response to 8 weeks of high-fat diet. (a) *En face* segment of aortic arch. Gross pathology revealed atherosclerotic lesions on the endoluminal surface. (b) *En face* segment from the descending aorta. Small lesions with a diameter less than 1 mm were present proximal to the aortic arch. The remaining endoluminal surface was grossly spared of visible lesion.

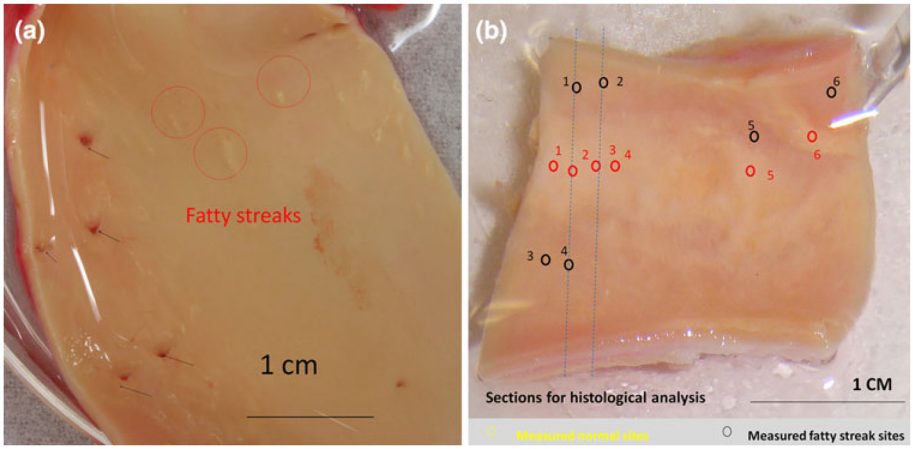

FIGURE 3.

Ex vivo segments of human descending thoracic aorta and common carotid artery. (a) *En face* thoracic aorta, revealing several orifices to the intercostal branches (black arrows) and fatty streaks (red circles) corresponding to the EIS readouts in Fig. 7a. (b) Numerous fatty streaks (red circles) and apparently normal endothelium (black circles) corresponded to the EIS readouts in Fig. 8a. Cross-sectional histological analyses were performed along blue dashed lines (Figs. 8c and 8d).

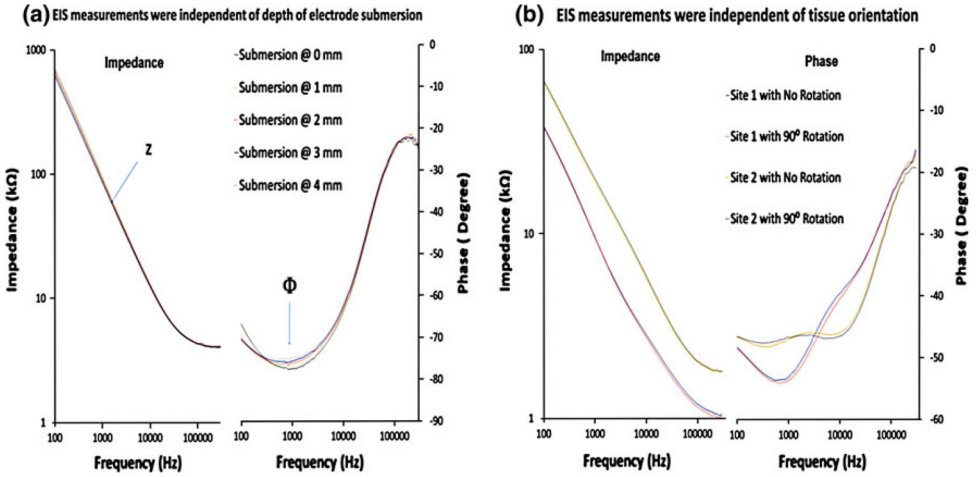

FIGURE 4.

EIS measurements in relation of the depth of microelectrode submersion and orientation of the specimens. (a) EIS and phase data of rabbit artery tissue submerged in PBS solution. The lowest impedance was about 4000 Ω at 300 kHz (left panel). The corresponding phase value was close to −15° indicating that the impedance was mostly in the ohmic resistance range (right panel). (b) EIS and phase data were compared between two sites. The impedance and phase readings were independent of the orientation of the specimens.

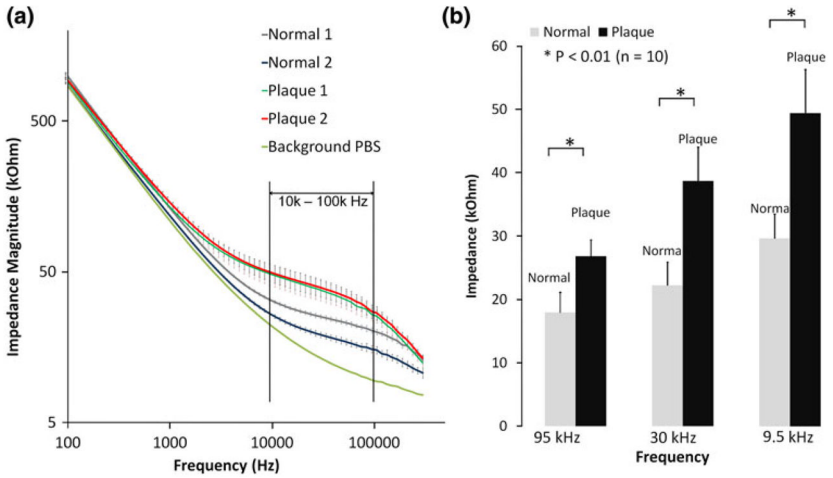

FIGURE 5.

Endoluminal EIS measurements in the aortic arch of NZW rabbits (a) EIS measurements were performed on 5 normal endoluminal sites and 5 plaque sites of the aortic arch tissue from two high-fat diet fed rabbits. Average impedance values at frequency range from 100 Hz to 300 kHz for healthy and plaque tissue from Rabbit 1 and Rabbit 2 were presented as Normal 1, Normal 2 (healthy tissue) and Plaque 1 and Plaque 2 (Plaque tissue), respectively (n = 5 for each group). Vertical bar denotes standard deviation. Baseline impedance measured from PBS solution alone was illustrated as a reference. (b) Differences in measured impedance from normal and plaque tissue were the most significant between operating frequency 10–100 kHz (* p<0.01, n = 10).

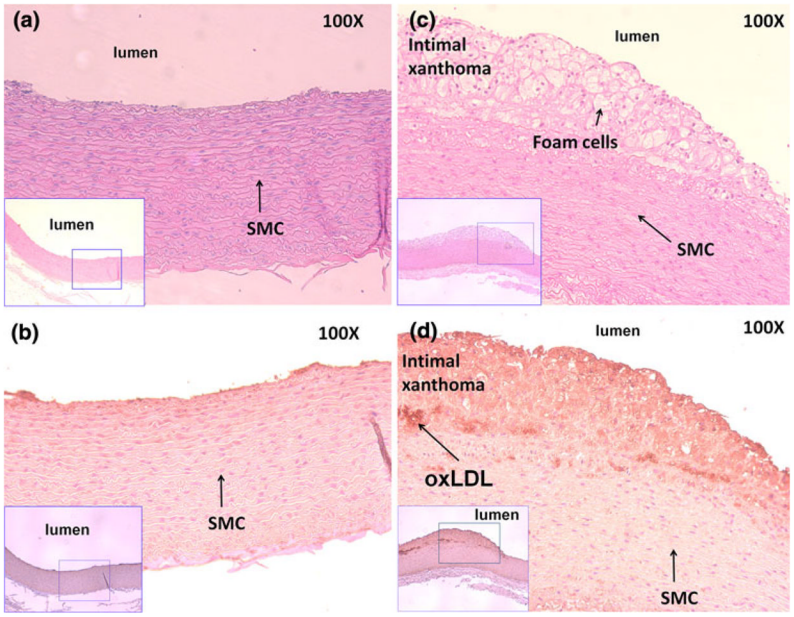

FIGURE 6.

Pre-atherosclerotic aortic arch lesions. (a) Aortic arch isolated from the rabbit on normal diet with absence of foam cells. (b) Corresponding immunohistochemical staining showed negative mAb4E6 stain for oxidized low density lipoprotein (oxLDL). (c) Intimal thickening and intimal xanthoma were prevalent in the aortic arch isolated from the rabbit with exposure to high-fat diet. Intimal thickening consists of mainly smooth muscle cells in a proteoglycan-rich matrix, whereas intimal xanthoma or otherwise known as a fatty streak primarily contains macrophage-derived foam cells, T lymphocytes, and varying degrees of smooth muscle cells (SMC). (d) Subendothelial layers were stained positive with mAb4E6 for oxLDL. Von Kossa staining was negative for calcification.

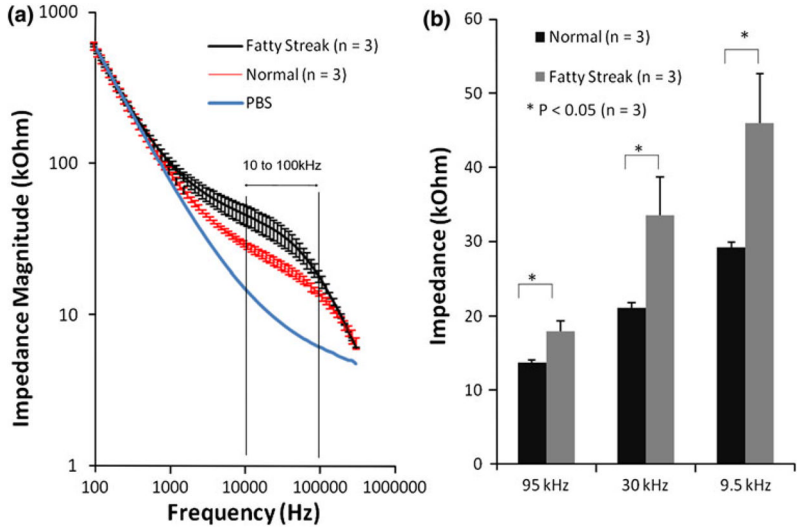

FIGURE 7.

Endoluminal EIS measurements from the human descending aorta. (a) EIS data results were performed on the thoracic aorta. Significantly higher impedance values were recorded from the fatty streaks over the frequency range from 10 to 100 kHz compared to the healthy endoluminal surface. (b) *T*-test verified the statistically significant difference in impedance measured at 95 kHz, 30 kHz, and 9.5 kHz between the healthy and plaque tissues (* $p < 0.05$, $n = 3$).

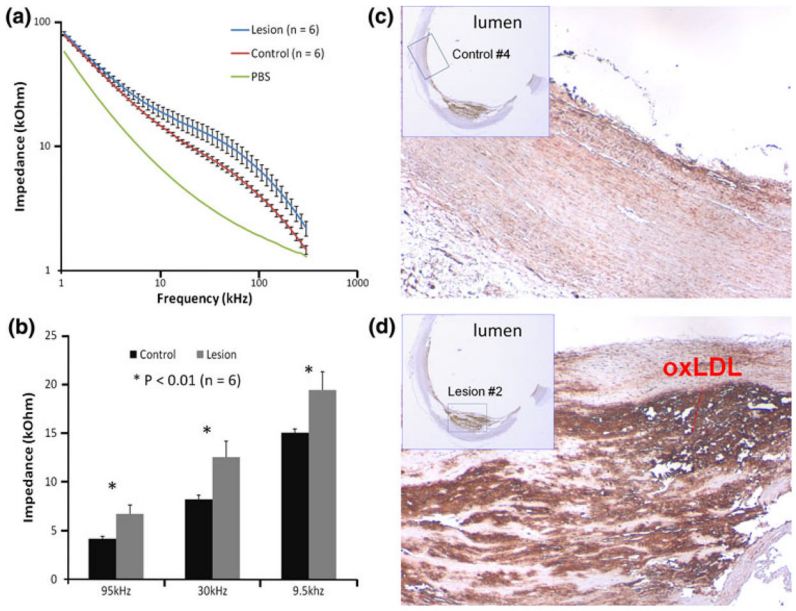

FIGURE 8.

EIS measurements in explants of human carotid arteries. (a) EIS measurements were performed on 6 control endoluminal sites and 6 lesion sites of human carotid arteries ($n = 6$). Average impedance values at frequency range 1000 Hz–300 kHz for control and lesion sites were presented as control vs. lesion, respectively ($n = 6$). Vertical bar denotes standard deviation. Baseline impedance measured from PBS solution alone was illustrated as a reference. (b) Differences in measured impedance from control and lesion sites were the most significant between operating frequency 10–100 kHz (* $p<0.01$, $n = 6$). (c) Immunohistochemistry was performed at the control site. (d) At the lesion site, subendothelial layers were stained positive with mAb4E6 for oxidized low density lipoprotein (oxLDL).